Experimental investigation of two-dimensional plasmons in a DySi$_2$ monolayer on Si(111)

E. P. Rugeramigabo,[1] T. Nagao,[2] and H. Pfnür[1],[*]

[1]*Institut für Festkörperphysik, Leibniz–Universität Hannover, 30167 Hannover, Germany*
[2]*Nano System Functionality Center, National Institute for Materials Science, 1-1 Namiki, Tsukuba 305-0044, Japan*
(Received 27 June 2008; published 1 October 2008)

DySi$_2$ monolayers were prepared by thermal evaporation of Dy at room temperature followed by annealing to 500 °C on Si(111), which yields a perfect (1×1) low-energy electron diffraction pattern. These monolayers of DySi$_2$ were investigated by electron energy loss spectroscopy with both high energy and momentum resolution. A low-energy acoustic-like dispersion was found with very small anisotropy in reciprocal space, consistent with the characteristic losses due to a two-dimensional plasmon in the hexagonal monolayer structure of DySi$_2$, and effective hole densities of $N_{2d} = 4.1 \times 10^{13}$ cm^{-2} with an effective mass of $m^* = 0.37 m_e$. Deviations of the expected dispersion due to single-particle excitations in the Si substrate were found above $q_\parallel = 0.08$ Å^{-1}. On (111) facets with terrace widths of 12 lattice constants, these properties change little along the terraces, but no plasmon wave propagation across step edges is possible, leading to strong suppression of characteristic loss signals in the direction normal to the steps.

I. INTRODUCTION

Plasmons in low-dimensional systems exhibit peculiar properties not existing in three dimensions. Due to the lack of a restoring force, two- and one-dimensional plasmons have an acoustic-like dispersion, i.e., their excitation energy goes to zero in the limit of large wavelengths.[1–4] Therefore, their properties differ strongly from surface plasmons on most bulk metals, which originate simply from the truncation of the bulk electronic system. However, several metal surfaces form partially filled two-dimensional (2D) surface states. Plasmons associated with these surface states are sufficiently decoupled from the three-dimensional (3D) electronic system so that they are also able to form 2D plasmons.[5]

Surface plasmons and their coupling to light is a field of strong recent interest because of many potential applications in conjunction with engineering cavity-free and broad band photon-emitter interactions[6] via subwavelength confinement of optical fields near metallic nanostructures.[6,7] The use of 2D plasmons, because of their strong dispersion compared with "conventional" surface plasmons, would allow an extreme confinement of light in a broad frequency range from medium to far infrared. In all cases, the group velocity of plasmons is many orders of magnitude lower than the speed of light, and coupling is only possible by use of appropriate nanostructures that supply the necessary momentum. Given that decay lengths over 100–1000 nm are expected,[5] conduction over reasonably long distances seems to be possible. This makes the search for appropriate low-dimensional metallic systems attractive that may be able to couple these excitations into electronic circuits.

Metallic monolayers (ML) on insulating surfaces are prototype materials for two-dimensional systems. Such layers on silicon surfaces play a key role, since they comprise a first step toward coupling of plasmons into electronic circuits. Especially silicide monolayers of rare-earth elements are very flexible systems. Depending on material combination and surface orientation, they both allow lattice matched iso-

tropic growth,[8–10] or, as on Si(100) surfaces, self-limiting and anisotropic growth as monolayer-thick nanowires[11–14] as well as adjustment of Schottky barriers.[15,16] 2D and one-dimensional (1D) plasmonics is a relatively new field, and only very few investigations have been carried out yet on the plasmons in such layers or wire structures.[4,17,18]

Before turning our interest to anisotropic structures, we report here as a first step on the plasmonic excitations and their properties on an isotropic monolayer of DySi$_2$ on Si(111). DySi$_2$ films are known to grow epitaxially with very small lattice mismatch on this surface.[19] Therefore, it is a prototype for an isotropic monolayer system. In the second part of the paper we show that plasmonic excitations can largely be suppressed by facet formation.

II. EXPERIMENT

Our experiments were carried out in an ultrahigh vacuum (UHV) chamber at a base pressure of 5×10^{-11} mbar equipped with a load lock system. The main measuring tool is a combination of a high resolution electron energy loss spectrometer (EELS) and with the deflection unit of a low-energy electron diffraction (LEED) system for spot profile analysis (SPA-LEED) for high-momentum resolution.[20] The electron source and the detector are fixed in this instrument so that the incident and the specularly reflected beam appear at an angle of 6° with respect to the surface normal. Although spectra of inelastically scattered electrons can be measured in the whole surface Brillouin zone (SBZ), all spectra reported here were taken close to the (00) beam for intensity reasons. With the apertures used here an energy resolution of about 10 meV can be achieved. While momentum resolution on Si surface can be tuned routinely below 1% SBZ, it depends for adsorbed layers on their quality. For the typical monolayer of DySi$_2$ used here in most of the experiments, we obtained a momentum resolution close to 1.5% SBZ for energies above 28 eV up to 100 eV.

As substrates we used Si samples cut from 300 μm-thick Si wafers manufactured, oriented, and polished on one side
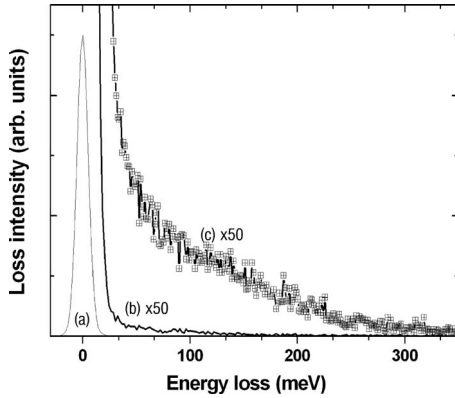
FIG. 1. Electron energy loss spectra of the clean Si(111) surface [curves (a) and (b)] and of 1 ML of DySi$_2$ at $q_{\parallel}=0$, showing the typical Drude tail of a metallic system [curve (c)]. Electron energy $E_p=47$ eV.

by Crystec (Berlin) in (111) and (111)4°[110] orientations. They were slightly p doped (conductivity at room temperature $>1000~\Omega$ cm). Metallic dysprosium was evaporated from a home-made thermal evaporator with water-cooled housing that also contained a quartz microbalance and a shutter for reproducible doses. During evaporation the Si samples were held at room temperature, and were annealed to 500 °C for 10 to 30 min before they were investigated with LEED either at room temperature or at 120 K. No significant differences in the measured results could be observed at the two measuring temperatures. The annealing step guarantees complete reaction of Dy to DySi$_2$ in the monolayer regime[19] and at the same time good ordering. The annealing temperature of 500 °C was chosen because the resulting structures are to a large extent independent of annealing time, in contrast, e.g., to annealing at 600 °C.

Coverages were calibrated also by using LEED, exploiting the fact that the monolayer of DySi$_2$ shows a perfect (1×1) structure. In the submonolayer regime a $2\sqrt{3} \times 2\sqrt{3}R30°$ structure is observed, which is followed by a (5×2) structure. Depending on the annealing temperature, a variable range of coexistence is found. Above one monolayer, a $\sqrt{3} \times \sqrt{3}R30°$ structure develops. Increasing coverage in steps between 0.05 and 0.1 ML, we observed the gradual disappearance of the submonolayer structures and finally the appearance of the multilayer $\sqrt{3} \times \sqrt{3}R30°$ structure. As it turned out, the pure (1×1) structure appears only in a small coverage window of ± 0.05 ML and thus allows a quite precise coverage calibration.

III. RESULTS

A. DySi$_2$ on flat Si(111)

Only close to completion of the monolayer, as indicated by the formation of a (1×1) structure without any traces of other structures even after repeated annealing, a conducting layer was detected when measuring electron energy loss spectra. The typical sign is the continuous and monotonically decreasing loss intensity known as the Drude tail of metallic systems. An example is shown in Fig. 1 at the Γ point of the
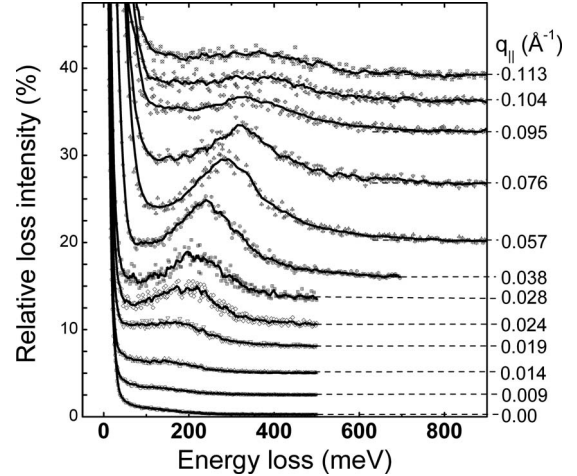

FIG. 2. HREELS spectra of 1 ML DySi$_2$ grown at room temperature and annealed to 500 °C. The spectra were taken at E_p $=38$ eV along the $\overline{\Gamma M}$ direction. Note that intensities are given relative to the elastic peak intensity, and that the curves were shifted against each other for clarity. Zero intensity is at the respective dashed lines.

Si(111) surface. Compared with clean Si(111), the loss intensity in the range between 50 and 200 meV is increased at least twenty times, clearly indicating the electronically conducting nature of the surface layer alone.

EEL spectra were now measured along high-symmetry directions $\overline{\Gamma K}$ and $\overline{\Gamma M}$ for a DySi$_2$ concentration of 1 ML at scattering angles deviating from the (00) beam. These scattering angles correspond to wave vectors $q_{\parallel} \neq 0$ parallel to the surface. An example is shown in Fig. 2 along the $\overline{\Gamma M}$ direction. As seen from this figure, a dispersing loss peak develops as a function of increasing $q_{\parallel}$. In the limit $q_{\parallel} \to 0$ it disappears in the Drude tail. At values of $q_{\parallel} > 0.06$ Å^{-1} the intensity decreases again, and is no longer detectable as one clear loss peak above $q_{\parallel}=0.12$ Å^{-1}. At the same time the peak broadens significantly.

This peak is energetically clearly outside the range of any vibrational excitations. It cannot be caused by the continuum of single-particle electronic excitations in a metallic system either (which is the origin of the Drude tail, but not of peaks with well-defined q values). It therefore must be attributed to collective excitations of the conduction electrons of the DySi$_2$ layer, i.e., to its plasmons.

Indeed, the loss peaks are strictly located at the surface as demonstrated by Fig. 3. Here we have carried out loss measurements at three different electron energies for fixed values of $q_{\parallel}$ thus varying the elastic mean free path of the electrons. Apart from a small reduction of intensity at higher energies, as expected, no changes of peak shapes or shifts were found. The loss peaks depend only on $q_{\parallel}$.

We now inspect details more closely. For this purpose, we fitted the loss spectra by first parametrizing the form of the elastic peak and the Drude tail taking spectra at $q_{\parallel}=0$ as reference. In the actual fit, a Voigt function was used for the loss peak with the relative contribution of Gauss and Lorentz function, the total widths and the total intensity as free parameters. The intensities of the elastic peak and of the Drude
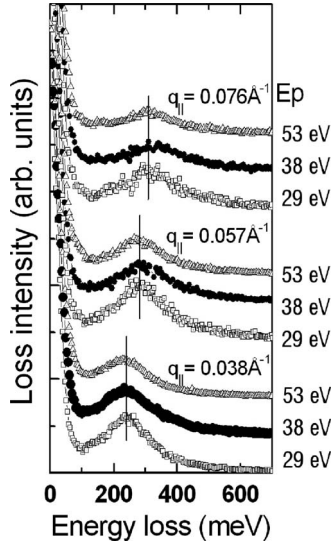
FIG. 3. Loss peaks measured at different electron energies, i.e., at various elastic mean free paths. Only a dependence on $q_\parallel$ is seen.

tail were additional free parameters. In Fig. 4, the peak positions of the loss peaks, i.e., their energy dispersion is plotted as a function of $q_\parallel$. These data are obviously compatible with an extrapolation to zero loss energy at $q_\parallel=0$. This demonstrates the acoustic nature of the plasmon losses and their two-dimensional character, as expected. Within the scatter of data, no clear anisotropy is found between the data in $\overline{\Gamma K}$ and $\overline{\Gamma M}$ directions (pointing toward the corners and the side centers of the hexagonal SBZ, respectively). Only at $q_\parallel < 0.015$ Å^{-1} these are true uncertainties of a small signal on a nonflat background. For higher $q_\parallel$ values, however, the scatter is more between different data sets, taken at a particular layer, than within a data set, i.e., the dispersion curves as a whole vary slightly. This effect is most likely due to small
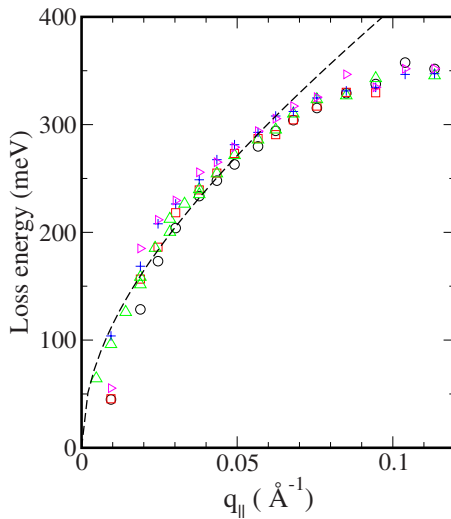

FIG. 4. (Color online) Dispersion of the plasmon losses measured in $\overline{\Gamma M}$ ($\square$, $\triangle$, $\triangleright$) and $\overline{\Gamma K}$ directions ($\bigcirc$, $+$) at electron energies of 53, 38, and 29 eV. Different symbols mark different data sets. A fit according to Eq. (1) is drawn as dashed line with $N_{2D}=9\times10^{13}$ cm^{-2} and $m^*=0.8m_e$.

variations of silicide concentration for several freshly prepared $DySi_2$ layers. These variations are coupled to the electron concentration. Since the $DySi_2$ layer has hexagonal symmetry, the small anisotropy is more or less expected. On the other hand, it is an indication for an epitaxial and undistorted crystalline growth of the $DySi_2$ layer.

In order to get an estimate for the effective electron density involved in formation of the 2D plasmons, we use the approximation of a nearly free 2D electron gas on the semi-infinite Si surface taken as a dielectric medium. Within second order, the dispersion should then be given by[2,4]

$$\omega^2(q_\parallel) = \frac{e^2}{\epsilon_0(1+\epsilon_{Si})}\frac{N_{2D}}{m^*}|q_\parallel| + 6\hbar^2\pi\frac{N_{2D}}{(2m^*)^2}q_\parallel^2 + \dots . \quad (1)$$

Here $\omega(q_\parallel)$ is the plasmon frequency, ϵ_{Si} the relative dielectric constant of Si taken as 11.5, N_{2D} the two-dimensional density of charge carriers responsible for the plasmon formation, m^* the effective mass, m_e the free electron mass, and $q_\parallel$ the plasmon wave vector. This function yields a reasonable fit to the data only for $q_\parallel < 0.07$ Å, whereas for higher $q_\parallel$ values the data are systematically below the fitting curves irrespective of the values chosen for N_{2D} and m^* (an example calculated with $N_{2D}=9\times10^{13}$ cm^{-2} and $m^*=0.8m_e$ is shown in Fig. 4 as dashed curve). Since Eq. (1) is most sensitive to the ratio N_{2D}/m^*, only this ratio can be safely determined. In units of 10^{14} cm^{-2} for N_{2D} and m^* in units of m_e a ratio of 1.1 ± 0.1 is obtained. The absolute concentration of charge carriers must therefore be determined from other data, e.g., from photoemission. The dispersion curves for this system[21] are virtually identical to those of $ErSi_2$.[22] This means that there is a nearly filled conduction band and six electron "pockets" around the $\bar{M}$ points, so that the electron concentration is equal to the hole concentration. From the estimation of curvatures it is evident that the effective electron mass is much larger than the effective hole mass[17,21] so that the plasmon excitation is mainly determined by the hole concentration. Let us assume that the hole concentration is solely responsible for the observed plasmon losses. The effective hole concentration is given by the Fermi wave vector, q_F, as determined from photoemission.[17,22] For the two-dimensional system $N_{2D}=q_F/2\pi$ results in $N_{2D}=4.1\times10^{13}$ cm^{-2}, and we obtain from our experimental data an effective mass of $0.37m_e$. This effective mass is smaller than that given in Ref. 17 but taking into account the uncertainties in the determination of effective masses of holes from photoemission,[21] the agreement is reasonable. It shows that our interpretation that we observe here mainly plasmons from a hole plasma is consistent.

Although the plasma oscillation of a 2D plasmon is longitudinal in character, the electric fields associated with this excitation have both longitudinal and transversal components. The coupling to the transversal component of the electric field by the impinging electrons leads to the characteristic dipole lobe of the inelastically scattered intensity, as shown in Fig. 5. In this figure we plotted the peak intensities of the plasmon losses as a function of $q_\parallel$ for three different energies for the incident electrons. All three curves show a
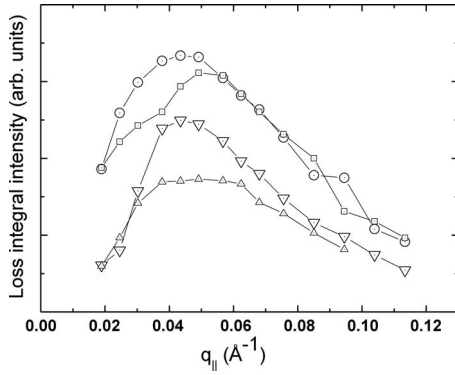
FIG. 5. Integrated loss intensities as a function of $q_\parallel$. Different symbols mark experimental data sets measured with incident electron energies of 29 eV ($\bigcirc$ and $\square$), 38 eV ($\triangledown$), and 53 eV($\triangle$).

maximum close to $q_\parallel=0.04$ Å^{-1}, and strong damping above $q_\parallel=0.08$ Å^{-1}.

The strong damping of intensities is also reflected in the full widths at half maximum (FWHM) as shown in Fig. 6 of the loss peaks. Here the slope clearly increases above a $q_\parallel$ value of 0.08 Å^{-1}. Both findings correlate with the deviation of the 2D plasmon fit from the measured data in Fig. 4. This additional damping may be due to single-particle excitations both in the silicide films and/or in the Si substrate. Interestingly, this damping mechanism is absent in our recent data of DySi$_2$ nanostripes on vicinal Si(001),[23] which have virtually the identical geometric structure within the silicide film. This means that their internal excitation spectrum should be very similar to the films investigated here. In contrast, the interface to Si(001) due to its different symmetry has a strongly different band structure compared with Si(111). Therefore, we conclude that the damping for $q_\parallel > 0.08$ Å^{-1} is mainly due to single-particle excitations at the Si(111) interface.

The half widths plotted in Fig. 6 are monotonously decreasing with decreasing $q_\parallel$ with a minimum of 170 meV at 0.028 Å^{-1}. This large minimal half width is not due to the short lifetime of the plasmons, but mainly an effect of integration in momentum space. The LEED spots in presence of the DySi$_2$ layer have a FWHM of 1.5% SBZ, corresponding to 0.03 Å^{-1}. Close to the minimum this corresponds to an averaging in energy space over 150 meV (see Fig. 4). In

other words, the measured width of the plasmon peaks at small $q_\parallel$ is mainly determined by the quality of the films and the instrumental resolution in q space, where in this case the effect of film quality dominates. Assuming Gaussian line shapes for both the "instrument" and the natural width, we get an upper estimate for the energetical plasmon widths at $q_\parallel=0.03$ Å^{-1} of 50 to 70 meV. Therefore, also the observed minimum is an instrumental effect due to the increasing slope of the plasmon dispersion curve at $q_\parallel \to 0$. This integration effect gets smaller with increasing $q_\parallel$, and does not dominate the FWHM any more above $q_\parallel=0.06$ Å^{-1}.

Indeed, plasmons cannot decay into single-particle excitations (SPE) as long as the plasmon dispersion curve does not enter the SPE continuum.[5,24] Therefore, an energy dependence of the excitation line width for plasmons much lower than $\propto E^2$ is expected[24] as long as SPEs are not possible. This was indeed found in experimental data of the Ag monolayer on Si(111),[4] of Au wires on Si(557),[18] and of DySi$_2$ wires on stepped Si(001).[23] In all these cases a dependence of the line width $\propto E^\alpha$ with α between 0.5 and 1 was found outside the region of SPE with a strong increase in slope and corresponding decay of peak intensities of loss peaks once SPE was possible. The observed plasmon decay in the former region was explained by multiple electron-hole excitations and by electron scattering.[3,4] A quadratic increase in the line widths on the excitation energy is indeed observed above $q_\parallel=0.08$ Å^{-1}, where the q-integration effect plays a negligible role, i.e., we get an approximately linear relationship on $q_\parallel$, as shown as dashed line in Fig. 6. While it presents the upper limit for the natural line widths of plasmon losses at small $q_\parallel$, it shows that single-particle excitations are the likely decay mechanism above $q_\parallel=0.08$ Å^{-1}. This seems to be consistent with semiquantitative calculations for ErSi$_2$ layers on Si(111).[25]

This short discussion was aimed to point out first the necessity for highly q-resolved measurements (apart from the necessary energy resolution) for reliable determinations of plasmon dispersion curves. Otherwise the integration in q space can never be reduced to a tolerable limit and makes a dispersion measurement at small q impossible. Even if the instrumental is sufficient, the film quality is of essential importance for the reliable determination of 2D and 1D plasmon excitations.

B. Faceted surfaces

Indeed, the quality of the surface strongly affects the development of a plasmon dispersion and its detectability, as we will demonstrate below. For this purpose, we prepared a (partly) faceted Si(111) sample by strong inhomogeneous heating. The resulting facets are uniaxially oriented along the $\overline{\Gamma M}$ direction (marked by c in Fig. 7). In plots of $q_\perp$ (momentum component normal to the surface) versus $q_\parallel$ we determined the preferential inclination angle with respect to the (111) direction of the facet rods in an Ewald construction (not shown) to be 4.37°. This is close to a (11 13 13) orientation with a rather wide distribution, however, as judged from the streaky appearance of the facet spots in Fig. 7. The preferred orientation corresponds to an average terrace width of 12 2/3 Si atoms.
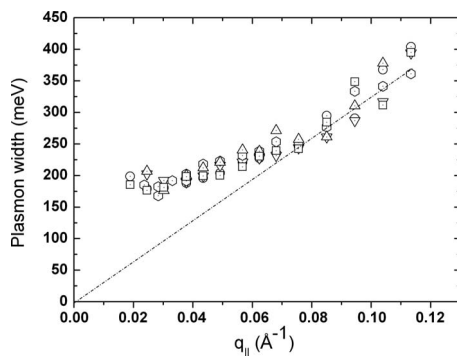

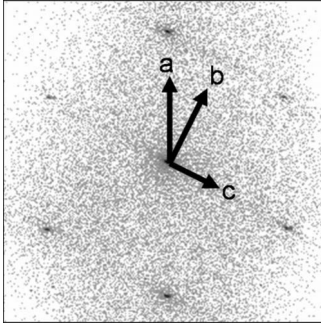FIG. 6. Full widths at half maximum as a function of $q_\parallel$. The line would be the result for lifetime broadening assuming a $1/E^2$ dependence of the lifetime.

FIG. 7. LEED pattern of a monolayer of DySi$_2$ on a faceted Si(111) surface.
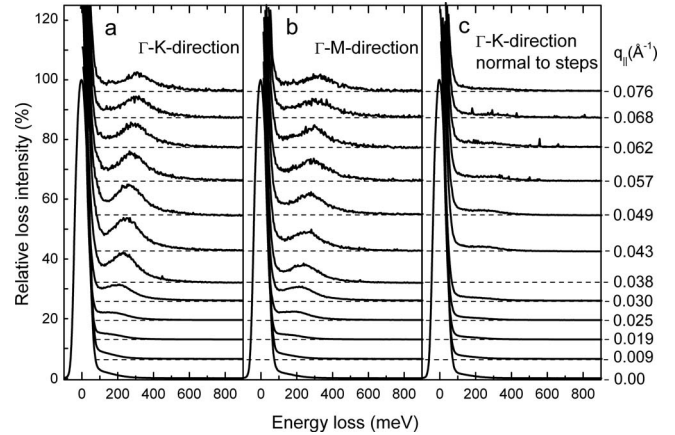

FIG. 8. Dispersion of 1 ML DySi$_2$ on a faceted Si(111) surface. The three data sets denoted (a), (b), and (c) correspond to the directions marked in Fig. 7 by the same letters. Levels of zero intensity have been shifted for clarity to the dashed lines.

On this surface we prepared again 1 ML of DySi$_2$, which resulted in the LEED pattern shown in Fig. 7, and determined the plasmon losses with EELS. As seen in Fig. 8, the plasmon losses along the terraces (directions a and b of Fig. 7, $\overline{\Gamma M}$ and $\overline{\Gamma K}$ directions, respectively) are essentially unchanged with respect to the flat Si(111) surface. In the direction normal to the steps, however, a strong suppression is seen so that for the majority of spectra only a Drude tail remains.

These results suggest that steps cannot be crossed by traveling plasmon waves, and wave propagation happens only along the terraces. Therefore, normal to the steps only standing waves of plasmons can be formed with a maximum wavelength of twice the terrace width. Interestingly, there is a small nearly dispersionless peak, with its maximum close to 280 meV loss energy, visible in Fig. 8(c) for $q_{\parallel}$ values above 0.04 Å^{-1}. It disappears in the Drude background at smaller values of $q_{\parallel}$. This peak may be an indication for the excitation not of the fundamental, but of the first excited mode of the standing waves. (The fundamental mode is predicted to have zero loss energy in the limit $q_{\parallel}=0$.)[26] Indeed for the given average strip width of 4.2 nm, this value is quite reasonable, as estimated from a simple particle-in-a-box model. Also, the excitation probability is expected to be higher for more asymmetric scattering geometries,[26] in agreement with our findings.

IV. SUMMARY AND CONCLUSIONS

Our momentum-resolved energy loss experiments allowed the unique identification of the plasmon dispersion in a two-dimensional DySi$_2$ monolayer. Comparison with photoemission data and the determination of the electron densities at E_F from there[22] show that the plasmonic excitations in this system can consistently be described by a hole plasmon gas with an effective mass close to $0.4m_e$. While damping by single-particle excitations sets in for high $q_{\parallel}$ values already for $q_{\parallel} > 0.08$ Å^{-1}, the half widths measured at $q_{\parallel} \rightarrow 0$ are mainly determined by the instrumental q resolution, i.e., by the integration radius in $q_{\parallel}$ space.

Not surprisingly, dispersion measurements are sensitive to structural and ordering properties of the surface layer. This is demonstrated by uniaxial faceting of the Si(111) surface. While the plasmon dispersion for DySi$_2$ along the facet terraces remains virtually unchanged compared with the DySi$_2$ layer on flat Si(111), we find no dispersion in the perpendicular direction. The remaining small loss peak found in this direction, with the $q_{\parallel}$ component along the terraces set to zero, is consistent with the excitation of the second harmonic standing wave expected for the plasmons on metallic stripes that are not directly in contact with each other.

*Corresponding author. pfnuer@fkp.uni-hannover.de

[1] S. J. Allen, D. C. Tsui, and R. A. Logan, Phys. Rev. Lett. **38**, 980 (1977).

[2] F. Stern, Phys. Rev. Lett. **18**, 546 (1967).

[3] T. Inaoka, T. Nagao, S. Hasegawa, T. Hildebrandt, and M. Henzler, Phys. Rev. B **66**, 245320 (2002).

[4] T. Nagao, T. Hildebrandt, M. Henzler, and S. Hasegawa, Phys. Rev. Lett. **86**, 5747 (2001).

[5] B. Diaconescu *et al.*, Nature (London) **448**, 57 (2007).

[6] A. V. Akimov, A. Mukherjee, C. L. Yu, D. E. Chang, A. S. Zibrov, P. R. Hemmer, H. Park, and M. D. Lukin, Nature (London) **450**, 402 (2007).

[7] D. E. Chang, A. S. Sørensen, P. R. Hemmer, and M. D. Lukin, Phys. Rev. Lett. **97**, 053002 (2006).

[8] P. Paki, U. Kafader, P. Wetzel, C. Pirri, J. C. Peruchetti, D. Bolmont, and G. Gewinner, Phys. Rev. B **45**, 8490 (1992).

⁹S. Vandré, T. Kalka, C. Preinesberger, and M. Dähne-Prietsch, J. Vac. Sci. Technol. B **17**, 1682 (1999).

¹⁰Z. He, D. J. Smith, and P. A. Bennett, Appl. Phys. Lett. **86**, 143110 (2005).

¹¹C. Preinesberger, S. Vandré, T. Kalka, and M. Dähne-Prietsch, J. Phys. D **31**, L43 (1998).

¹²D. Lee, D. K. Lim, S. S. Bae, S. Kim, R. Ragan, D. A. A. Ohlberg, Y. Chen, and R. S. Williams, Appl. Phys. A: Mater. Sci. Process. **80**, 1311 (2005).

¹³C. Preinesberger, G. Pruskil, S. K. Becker, M. Dähne, D. V. Vyalikh, S. L. Molodtsov, C. Laubschat, and F. Schiller, Appl. Phys. Lett. **87**, 083107 (2005).

¹⁴H. W. Yeom, Y. K. Kim, E. Y. Lee, K.-D. Ryang, and P. G. Kang, Phys. Rev. Lett. **95**, 205504 (2005).

¹⁵H. Norde, J. de Sousa Pires, F. d'Heurle, F. Pesavento, S. Petersson, and P. A. Tove, Appl. Phys. Lett. **38**, 865 (1981).

¹⁶S. Vandré, T. Kalka, C. Preinesberger, and M. Dähne-Prietsch, Phys. Rev. Lett. **82**, 1927 (1999).

¹⁷T. Angot and G. Gewinner, J. Electron Spectrosc. Relat. Phenom. **104**, 173 (1999).

¹⁸T. Nagao, S. Yaginuma, T. Inaoka, and T. Sakurai, Phys. Rev. Lett. **97**, 116802 (2006).

¹⁹I. Engelhardt, C. Preinesberger, S. K. Becker, H. Eisele, and M. Dähne, Surf. Sci. **600**, 755 (2006).

²⁰H. Claus, A. Büssenschütt, and M. Henzler, Rev. Sci. Instrum. **63**, 2195 (1992).

²¹M. Wanke, K. Löser, G. Pruskil, and M. Dähne, J. Appl. Phys. **103**, 094319 (2008).

²²P. Wetzel, C. Pirri, P. Paki, J. C. Peruchetti, D. Bolmont, and G. Gewinner, Solid State Commun. **82**, 235 (1992).

²³E. P. Rugeramigabo, T. Nagao, and H. Pfnür (unpublished).

²⁴V. M. Silkin, J. M. Pitarke, E. V. Chulkov, and P. M. Echenique, Phys. Rev. B **72**, 115435 (2005).

²⁵L. Stauffer, A. Mharchi, C. Pirri, P. Wetzel, D. Bolmont, G. Gewinner, and C. Minot, Phys. Rev. B **47**, 10555 (1993).

²⁶T. Inaoka, Phys. Rev. B **71**, 115305 (2005).